



Anisotropic Contraction of Fiber-Reinforced Hydrogels

Journal:	<i>Soft Matter</i>
Manuscript ID	SM-ART-06-2018-001251.R2
Article Type:	Paper
Date Submitted by the Author:	31-Aug-2018
Complete List of Authors:	Liu, Shuangping; Northwestern University, Materials Science and Engineering Stupp, Samuel; Northwestern University, Olvera de la Cruz, Monica; Northwestern University, Materials Science and Engineering

Cite this: DOI: 10.1039/xxxxxxxxxx

Anisotropic Contraction of Fiber-Reinforced Hydrogels[†]

Shuangping Liu,^a Samuel I. Stupp,^{abc} and Monica Olvera de la Cruz^{*abd}Received Date
Accepted Date

DOI: 10.1039/xxxxxxxxxx

www.rsc.org/journalname

Hydrogels reinforced by fibers can undergo remarkable anisotropic contraction triggered by external stimuli, which has a broad appeal for various applications. However, little is known about how to optimize the contraction anisotropy by tuning the microstructures of fiber-reinforced hydrogels. Here, we investigate the underlying mechanisms controlling the anisotropic contraction of fiber-reinforced hydrogels. Using a simplified model incorporating the directional constraint of the fibers, we show that the contraction anisotropy can be substantially enhanced if the hydrogel is prestretched along the fiber direction. We further explicitly model fibers as periodically distributed cylindrical rods in the finite element simulations, and find that the contraction anisotropy can be maximized by varying the transverse fiber-fiber distance; this maximum anisotropy can be improved by reducing the longitudinal fiber-fiber distance and increasing the fiber length. Our study provides insights into designing novel fiber-reinforced hydrogels, suggesting possible applications in soft robotics, tissue engineering and beyond.

1 Introduction

Hydrogels, which can undergo dramatic volumetric changes in response to diverse stimuli such as temperature, pH, light and electric field^{1,2}, have emerged in a broad range of applications in tissue engineering³, soft robotics^{4,5}, drug delivery⁶, intelligent biosensors^{7,8}, and 3D printing⁹. In particular, great attention is being focused on developing hydrogels with anisotropic mechanical properties that can be utilized to mimic a variety of biological tissues with anisotropic morphologies, including cornea¹⁰, skins¹¹, striated muscles^{12,13} and articular cartilages^{14,15}. Anisotropic hydrogels are also exploited for the fabrication of soft robotic actuators to trigger unidirectional motion¹⁶; in 3D printing, the anisotropic swelling of the hydrogel-based ink is critical to transform 2D patterns into the desired 3D shapes⁹. Thus designing hydrogels with ordered microstructures that impart controllable anisotropic mechanical properties is of both theoretical and experimental interest.

Previous research has reported diverse microstructures that en-

dow the isotropic hydrogels with anisotropic mechanical behaviors. For example, carbon nanotubes have been aligned in an otherwise isotropic hydrogel matrix using dielectrophoresis to generate both mechanical and electrical anisotropy¹⁷. Charged titania nanosheets can be cofacially oriented as layered structures which resist the hydrogels to shrink along the orthogonal direction to the sheets¹⁶. More types of microstructural morphologies including lamellar¹⁸, porous¹⁹ and crystalline structures²⁰ are also investigated in previous studies. In particular, hydrogels with fibrous microstructures have been extensively explored and commonly adopted in biomimetics to simulate many soft tissues^{11,13,14,21,22}. Remarkable anisotropic swelling and contraction of fiber-reinforced hydrogels have been reported in recent studies. Chin, *et al.* have fabricated the thermo-responsive tubular polymer hydrogel from a scaffold consisting of aligned self-assembled peptide amphiphile (PA) nanofibers; with specified temperature changes, the contraction strain perpendicular to the PA nanofibers is observed to be $\sim 100\%$ higher than that along the PA nanofibers²³. Similar anisotropy is also found in the swelling of the 3D printing ink based on hydrogels filled with aligned cellulose fibrils⁹.

The anisotropic swelling and contraction of fiber-reinforced hydrogels stem from the directional constraints enforced by the oriented fibers. In the homogenization-based constitutive models for anisotropic hydrogels²⁴, these constraints are incorporated as an energetic contribution with extra parameters defined to characterize the strength of the fiber reinforcement. Previous studies following this approach have investigated the anisotropic

^a Department of Materials Science and Engineering, Northwestern University, Evanston, Illinois 60208, USA; E-mail: m-olvera@northwestern.edu

^b Department of Chemistry, Northwestern University, Evanston, Illinois 60208, USA

^c Simpson Querrey Institute for BioNanotechnology, Northwestern University, Chicago, Illinois 60611, USA

^d Department of Physics and Astronomy, Northwestern University, Evanston, Illinois 60208, USA

[†] Electronic Supplementary Information (ESI) available: [details of any supplementary information available should be included here]. See DOI: 10.1039/cXsm00000x/

swelling of fiber-reinforced hydrogels in various geometries such as thin sheets²⁵ and cylindrical tubes²⁶. However, fiber properties, such as their dimensions and distributions, are not available in these phenomenological models; such morphological information is necessary for experiments to fabricate hydrogels with desired anisotropy. In fact, it still remains poorly understood how to maximize the swelling and contraction anisotropy of hydrogels by tuning the underlying microstructures.

In this contribution, we aim to achieve an in-depth understanding of the mechanisms maximizing the anisotropic contraction of fiber-reinforced hydrogels. Based on the Flory-Rehner theory, we firstly inspect the contraction anisotropy of a uniaxially constrained hydrogel, a simplified model which retains the directional constraint of the fibers. An upper bound of the contraction anisotropy determined by the prescribed isotropic contraction ratio is discovered when the hydrogel is initially strain-free. We further investigate potential improvements of this upper bound by applying prestrains to the hydrogel. Our study reveals a remarkable enhancement of the contraction anisotropy when the uniaxially constrained hydrogel is prestretched along the constrained direction.

To examine the anisotropic contraction under the impact of the finite dimensions of fibers, we perform finite element simulations with periodic boundary conditions incorporated. By releasing the longitudinal restrictions of the fibers, maximum contraction anisotropies are identified when varying the transverse fiber-fiber distance. More approaches to improve the maximum anisotropy are noticed and explained, such as reducing the longitudinal fiber-fiber distance and increasing the fiber length. Our study provides new perspectives to control the anisotropic contraction of fiber-reinforced hydrogels, thus suggesting potential utilizations in designing novel anisotropic hydrogels for soft robotics, tissue engineering and biomedical devices.

2 Flory-Rehner theory

We describe the deformation and contraction of the hydrogel using the classical Flory-Rehner theory²⁷. The free energy of a hydrogel consists of the elastic energy of the polymer network and the polymer-solvent mixing energy:

$$F = F_{\text{el}} + F_{\text{mix}} \quad (1)$$

Various forms of elastic energy have been proposed in former research to characterize the reduction of entropy by stretching the cross-linked polymer network^{28–30}. In the present work, F_{el} follows the simplest form derived by Wall and Flory based on the Gaussian statistics²⁸:

$$F_{\text{el}}(\lambda_1, \lambda_2, \lambda_3, T) = \frac{1}{2} NkT \left[\lambda_1^2 + \lambda_2^2 + \lambda_3^2 - 3 - \ln(\lambda_1 \lambda_2 \lambda_3) \right] \quad (2)$$

where N is the number of polymer chain segments between the crosslinking junctions and $\lambda_1, \lambda_2, \lambda_3$ are the stretch ratios along the three principal axes in reference to the molten state of the polymer.

The polymer-solvent mixing energy F_{mix} is given by the Flory-

Huggins theory³¹

$$F_{\text{mix}}(\phi, T) = kT \frac{V}{v} [(1 - \phi) \ln(1 - \phi) + \chi \phi(1 - \phi)] \quad (3)$$

where V is the volume of the whole hydrogel, v is the volume of each solvent molecule, ϕ is the volume fraction of the monomers and χ is the Flory-Huggins interaction parameter between polymer chains and the solvent molecules. Let V_m be the volume of the polymer chains in the molten state, the volume fraction of the monomers is defined as

$$\phi = \frac{V_m}{V} = (\lambda_1 \lambda_2 \lambda_3)^{-1} \quad (4)$$

The free energy given in Eq. 2 and 3 allows us to analytically solve the equilibrium state of hydrogel for simple cases that are pivotal to our subsequent analysis. For an isotropic free-shrinking hydrogel, $\lambda_1 = \lambda_2 = \lambda_3 = \phi^{-1/3}$. When the gel is in equilibrium with the external solvent, the osmotic pressure $\Pi = -(\partial F / \partial V)_T = 0$, which gives

$$\chi = \frac{1}{2} \frac{Nv}{V_m} \left(\frac{1}{\phi} - \frac{2}{\phi^{5/3}} \right) - \frac{1}{\phi^2} \ln(1 - \phi) - \frac{1}{\phi} \quad (5)$$

If a uniaxial constraint is applied to an isotropic hydrogel along the longitudinal direction, the principal stress along the transverse directions should still vanish at thermodynamic equilibrium. Let $\lambda_{\perp} = \lambda_1 = \lambda_2$ be the transverse stretch ratio, and $\lambda_{\parallel} = \lambda_3$ be the longitudinal stretch ratio, then $\sigma_1 = \sigma_2 = (V_m \lambda_{\perp} \lambda_{\parallel})^{-1} (\partial F / \partial \lambda_{\perp})_{T, \lambda_{\parallel}} = 0$, which delivers

$$\chi = \frac{1}{2} \frac{Nv}{V_m} \left(\frac{1}{\phi} - \frac{2}{\phi^2 \lambda_{\parallel}} \right) - \frac{1}{\phi^2} \ln(1 - \phi) - \frac{1}{\phi} \quad (6)$$

The principal stress in the longitudinal direction σ_3 is written as

$$\sigma_3 = \frac{1}{V_m \lambda_{\perp}^2} \left(\frac{\partial F}{\partial \lambda_{\parallel}} \right)_{T, \lambda_{\perp}} = \frac{NkT}{V_m} \frac{\phi}{\lambda_{\parallel}} \left(\frac{1}{\phi_c} - \frac{1}{\phi} \right) \quad (7)$$

where $\phi_c = \lambda_{\parallel}^{-3}$ and Eq. 6 is used to eliminate χ . When $\phi = \phi_c$, $\sigma_3 = 0$, and Eq. 6 reduces to 5 due to the vanishing of the longitudinal constraint. In the following analysis, the uniaxial constraint applied to the hydrogel is described using the longitudinal strain ε_{\parallel} in reference to the isotropic free-shrinking state at the current χ :

$$\varepsilon_{\parallel} = \frac{\lambda_{\parallel} - \lambda}{\lambda} \quad (8)$$

where λ is the equilibrated stretch ratio of an isotropic free-shrinking hydrogel.

It is noteworthy that the derivation of Eq. 5 and 6 assumes that χ is independent of ϕ and only varies in response to the external stimuli. In practice, however, χ may depend on ϕ in certain polymer solutions³², which will be separately addressed later on in this paper.

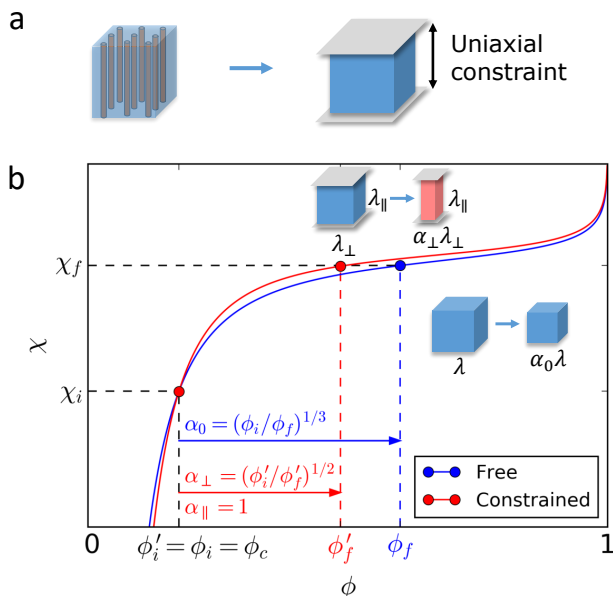


Fig. 1 Schematic plots of hydrogel contractions in response to increasing χ . (a) A fiber-reinforced hydrogel is simplified as a uniform hydrogel subject to a uniaxial constraint along the fiber direction. (b) The contraction of a free-shrinking hydrogel (blue curve) and a uniaxially constrained hydrogel (red curve) with a fixed λ_{\parallel} ($\alpha_{\parallel} = 1$). Both of the contractions start at the intersection point $\phi_i = \phi'_i = \phi_c = \lambda_{\parallel}^{-3}$. The arrows represent the direction of contractions along the ϕ axis.

3 Anisotropic contraction of a uniaxially constrained hydrogel

Based on the Flory-Rehner theory, we formulate a simplified model of fiber-reinforced hydrogels to explore the potential mechanisms enhancing the contraction anisotropy. Specifically, the anisotropic contraction of the aforementioned uniaxially constrained hydrogel is investigated in the absence of the oriented fibers (see Fig. 1a): in the longitudinal direction (parallel to the fiber direction) the contraction of the hydrogel is restricted, whereas in the transverse directions the hydrogel can shrink freely. Herein we essentially preserve the directional constraint from the fibers which apparently plays a critical role in the anisotropic contraction, and meanwhile eliminate the complex local deformations introduced by the fibers for simplicity.

In experiments, the anisotropic contraction of a hydrogel with non-trivial microstructures is often investigated and evaluated by comparing with the isotropic contraction of an unmodified hydrogel^{9,16,23}. Following this paradigm, we firstly imagine that a free hydrogel undergoes an isotropic contraction in response to an external stimulus which increases its Flory-Huggins parameter from χ_i to χ_f , as depicted by the blue curve in Fig. 1b. The stretch ratio of the hydrogel along each dimension is reduced from λ_i to λ_f , and correspondingly the volume fractions of the monomers increases from ϕ_i to ϕ_f according to Eq. 4. The contraction ratio along each principal axis, denoted by α_0 , can be defined as

$$\alpha_0 = \frac{\lambda_f}{\lambda_i} = \left(\frac{\phi_i}{\phi_f} \right)^{1/3} \quad (9)$$

In the following analysis, we assume that α_0 is prescribed by the external stimulus, allowing us to use α_0 as a benchmark to evaluate the anisotropic contraction of a uniaxially constrained hydrogel.

For a hydrogel uniaxially constrained along the longitudinal direction, it shrinks anisotropically if its χ increases from χ_i to χ_f . The contraction ratio along the longitudinal and transverse directions are denoted by α_{\parallel} and α_{\perp} respectively. We can likewise define the contraction ratio α_{\parallel} and α_{\perp} as

$$\alpha_{\parallel} = \frac{\lambda_{\parallel,f}}{\lambda_{\parallel,i}} \quad \alpha_{\perp} = \frac{\lambda_{\perp,f}}{\lambda_{\perp,i}} \quad (10)$$

where λ_{\parallel} is the longitudinal stretch ratio and λ_{\perp} is the transverse stretch ratio. The subscripts i and f represent the initial and shrunken state respectively. We define the contraction anisotropy A as

$$A = \frac{\alpha_{\parallel}}{\alpha_{\perp}} = \frac{\lambda_{\parallel,f} \lambda_{\perp,i}}{\lambda_{\parallel,i} \lambda_{\perp,f}} \quad (11)$$

Therefore, the larger A , the stronger the contraction anisotropy of the hydrogel.

Let ϕ'_i and ϕ'_f be the volume fractions of the monomers before and after the contraction; the contraction anisotropy A is bounded by the following inequality:

$$A = \frac{\lambda_{\parallel,f} \lambda_{\perp,i}}{\lambda_{\parallel,i} \lambda_{\perp,f}} = \left(\frac{\phi'_f}{\phi'_i} \right)^{1/2} \left(\frac{\lambda_{\parallel,f}}{\lambda_{\parallel,i}} \right)^{3/2} \leq \left(\frac{\phi'_f}{\phi'_i} \right)^{1/2} \quad (12)$$

Eq. 12 takes equality when $\alpha_{\parallel} = 1$ and $\alpha_{\perp} = (\phi'_i/\phi'_f)^{1/2}$, indicating that the anisotropy of the contraction is maximized when the hydrogel is not allowed to shrink along the longitudinal direction (i.e., λ_{\parallel} is constant). Using Eq. 5 and Eq. 6, we can evaluate the maximum contraction anisotropy $A_{\max} = (\phi'_i/\phi'_f)^{1/2}$ in terms of the prescribed increment of χ (or the isotropic contraction ratio α_0) and the initial strain state ε_{\parallel} of the hydrogel, which provides clues to improve the contraction anisotropy of the hydrogel.

3.1 Stress-free initial state

If the uniaxially constrained hydrogel starts to shrink from the stress-free state ($\phi'_i = \phi_i = \phi_c$, $\varepsilon_{\parallel} = 0$), we find that the maximum contraction anisotropy (A_{\max}) must be smaller than $\alpha_0^{-3/2}$. As illustrated in Fig. 1b, if $\phi'_i = \phi_i = \phi_c$, $\phi'_f < \phi_f$ for any $\chi_f > \chi_i$, i.e., the volumetric change of the uniaxially constrained hydrogel is always smaller than that of a free hydrogel, thus

$$A_{\max} = \left(\frac{\phi'_f}{\phi'_i} \right)^{1/2} < \left(\frac{\phi_f}{\phi_i} \right)^{1/2} = \alpha_0^{-3/2} \quad (13)$$

Eq. 13 can also be analytically proved by comparing Eq. 5 with 6 (see SI). Consequently, A_{\max} is upper bounded by $\alpha_0^{-3/2}$ if there is no prestrain involved in the initial state of the shrinking process.

Contraction experiments of fiber-reinforced hydrogels satisfying Eq. 13 have been reported in previous research. For example, in Chin *et al.*'s work²³, the tubular polymer gel shrank isotropically to 77% of its original size when the temperature ramped up from room temperature to $\sim 70^\circ\text{C}$, i.e., $\alpha_0 = 0.77$. If the gel

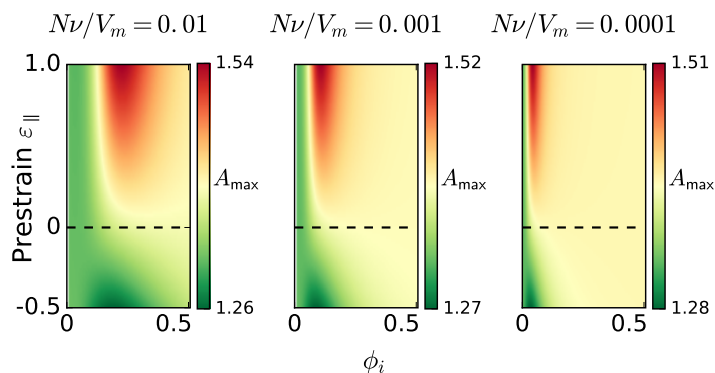


Fig. 2 Contraction of uniaxially constrained hydrogels with prestrain $\varepsilon_{\parallel} \neq 0$. The upper bound of the contraction anisotropy (A_{\max}) as a function of ϕ_i and ε_{\parallel} for different Nv/V_m . $\alpha_0 = 0.8$ in all subfigures. The longitudinally prestretched ($\varepsilon_{\parallel} > 0$) and precompressed ($\varepsilon_{\parallel} < 0$) states are separated by the dashed lines. ϕ_i is limited within the range $0 \sim 0.5$ because the final volume fractions ϕ_f and ϕ_f' must be less than 1 due to the specified α_0 .

was reinforced with circumferentially aligned peptide amphiphile nanofibers, the height and diameter of the tube shrank respectively to 62% and 80% of the original dimensions upon the same variation of temperature; the contraction anisotropy $A = 1.29$ is smaller than $\alpha_0^{-3/2} \approx 1.48$ within the margin of error ($|\Delta A| \approx 0.1$), which agrees with Eq. 13.

3.2 Prestrained initial state

If the uniaxially constrained hydrogel is prestrained before contraction ($\phi_i, \phi_i' \neq \phi_c, \varepsilon_{\parallel} \neq 0$), the upper bound suggested by Eq. 13 may not hold. For example, in supplementary Fig. S1, if $\phi_i' > \phi_c$, ϕ_i' and ϕ_i at the same χ_i no longer coincide with each other; it can be identified that at certain χ_i and χ_f , $\phi_f'/\phi_i' > \phi_f/\phi_i$ so that $A_{\max} > \alpha_0^{-3/2}$.

Indeed, our further analysis uncovers that A_{\max} can be significantly greater than $\alpha_0^{-3/2}$ if the hydrogel is longitudinally prestretched before contraction. Specifically, for an arbitrary ϕ_i , a prestrain within the range from -0.5 to 1.0 is applied to the free-swelling hydrogel so that ϕ_i' can be determined by equating Eq. 5 to Eq. 6 and meanwhile incorporating Eq. 8. By setting $\alpha_0 = 0.8$, we numerically calculate A_{\max} for different Nv/V_m . Results (see Fig. 2) clearly reveal that A_{\max} can be larger than $\alpha_0^{-3/2} \approx 1.40$ only when $\varepsilon > 0$. For example, for $Nv/V_m = 0.01$, A_{\max} can be as large as 1.54 when $\varepsilon_{\parallel} = 1.0$. The value of A_{\max} becomes larger as a whole when ε increases, and eventually converges to $(\phi_i')^{-1/2}$ when the hydrogel volume V approaches V_m . In addition, the distribution patterns of A_{\max} in Fig. 2 demonstrate a significant shift when Nv/V_m reduces. Since Nv/V_m is only associated with the elastic terms in Eq. 2, our observation implies that initially more swollen states are favored to produce stronger contraction anisotropy when the hydrogel is less rigid. In conclusion, the contraction anisotropy of a uniaxially constrained hydrogel can be substantially stronger if the hydrogel is longitudinally prestretched.

For a realistic fiber-reinforced hydrogel, the prestretching condition may be potentially realized in several approaches. The

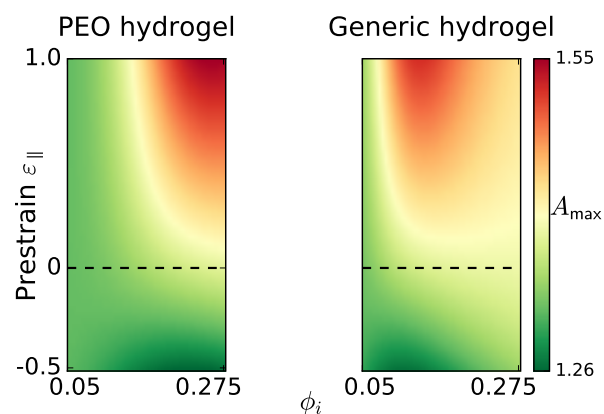


Fig. 3 Contraction of PEO hydrogels upon increasing temperature. The upper bound of the contraction anisotropy (A_{\max}) as a function of ϕ_i and ε_{\parallel} for a PEO hydrogel (left) and a generic hydrogel with ϕ -independent χ (right). $Nv/V_m = 0.002$ and $\alpha_0 = 0.8$ in all subfigures.

simplest approach is to apply an external control to the hydrogel along the fiber direction. Prestretching may also be introduced if the fiber-reinforced hydrogel is already in the shrunken state before performing the contraction experiments. Additionally, incorporating the fibers into the hydrogel matrix may lead to intrinsic prestretching due to the interaction between the fibers and the polymer chains.

3.3 ϕ -dependent χ

If χ varies as a function of ϕ , an explicit dependence of χ on both the stimulus intensity (denoted by T) and ϕ is required to analyze the contraction of hydrogels through the above approach. In previous discussions, we have assumed that χ is independent of ϕ , therefore the external stimulus and the deformation are naturally decoupled in Eq. 5 and 6, which allows us to investigate the contraction behaviors without knowing the specific form of $\chi(T)$. In contrast, if χ also depends on ϕ , we need to replace χ with $\bar{\chi}$ in Eq. 5 and 6:

$$\bar{\chi} = \chi - \phi \frac{\partial \chi}{\partial \phi} \quad (14)$$

With the knowledge of the function $\chi(T, \phi)$, the relation between T and ϕ at equilibrium can be obtained and exploited to investigate the contraction behaviors.

To exemplify the above procedure for handling the ϕ -dependent χ , we analyze the contraction behaviors of a crosslinked poly(ethylene oxide) (PEO) hydrogel, a widely used thermoresponsive polymer with both upper and lower critical solution temperature phase behaviors³³. The free energy of PEO in aqueous solutions can be formulated using the Dormidontova's model³⁴, which incorporates the free energy of both the PEO-water and water-water hydrogen bondings to successfully explain the unique phase behaviors of PEO/water solutions. Based on $\bar{\chi}(T, \phi)$ derived from the Dormidontova's model (see supplementary Eq. S9; here T represents temperature), we numerically calculate the $T \sim \phi$ relation for both the free-shrinking and uniaxially constrained condition, as shown in supplementary Fig. S2. Given a stimulus of temperature $T_i \rightarrow T_f$, we imagine that a free-

shrinking PEO hydrogel undergoes an isotropic contraction from ϕ_i to ϕ_f with a contraction ratio of α_0 along each dimension, while a uniaxially constrained PEO hydrogel with a longitudinal pre-strain ε_{\parallel} shrinks from ϕ'_i to ϕ'_f . In a similar way as Fig. 2, we calculate A_{\max} for $-0.5 \leq \varepsilon_{\parallel} \leq 1.0$ and $0.050 \leq \phi_i \leq 0.275$ at a specified α_0 (see Fig. 3). Using the same set of parameters, a similar diagram for a generic hydrogel with ϕ -independent χ is also constructed within the same range of ε_{\parallel} and ϕ_i for comparison purposes.

Results in Fig. 3 clearly indicate that the ϕ -dependent χ of PEO hydrogel alters the anisotropic contraction behavior by shifting the maximum of A_{\max} within the inspected range of ϕ and ε_{\parallel} . However, the prestretching mechanism to enhance the contraction anisotropy still works for PEO hydrogel: A_{\max} can be larger than $\alpha_0^{-3/2}$ only when $\varepsilon_{\parallel} > 0$.

4 Anisotropic contraction of fiber-reinforced hydrogels: finite element simulations

The finite dimensions of the fibers, which are absent in previous discussions, can introduce more complexity to the anisotropic contraction of hydrogels. Besides the inhomogeneous strain field around the fibers, compact packing of the oriented stiff fibers within a hydrogel may also dampen the overall contractions along the transverse directions. Meanwhile, the finite length of the fibers allows the hydrogel to shrink along the longitudinal direction instead of being completely constrained. As a result, the anisotropic behavior of the hydrogel significantly deviates from a uniaxially constrained hydrogel when the fibers have finite dimensions. Unfortunately, analytical solutions are difficult to obtain when the fibers are included in the model. Various approaches have been proposed in former research for numerical simulations of hydrogels^{35–39}. In particular, the finite element method is well suited for understanding swelling hydrogels in complex geometries such as wrinkling, creasing, and other intriguing buckled structures^{40–43}. Therefore, we resort to the finite element method to explore the anisotropic contraction of a fiber-reinforced hydrogel in the following sections.

4.1 Model geometry and boundary conditions

In our simulations, each fiber is modeled as a rigid cylinder with diameter d and length l attaching to the surrounding hydrogel matrix without allowing any relative sliding (see Fig. 4, top left). The ends of each fiber are smoothed with semi-spherical cups to avoid singular stress concentration at sharp corners. We arrange the fibers periodically within the hydrogel so that periodic boundary conditions can be applied to the model. Specifically, the periodic array of fibers and their surrounding hydrogel are described as identical unit cells spanned by a set of lattice vectors ($\mathbf{a}, \mathbf{b}, \mathbf{c}$). Let S and S' be the opposite faces along the direction of \mathbf{c} (see Fig. 4, bottom), $\mathbf{u}(\mathbf{r})$ represent the displacement of an arbitrary point located at \mathbf{r} on S (thus $\mathbf{u}(\mathbf{r} + \mathbf{c})$ lies on S'), and ($\mathbf{a}', \mathbf{b}', \mathbf{c}'$) denote the lattice vectors after deformation; the periodic boundary

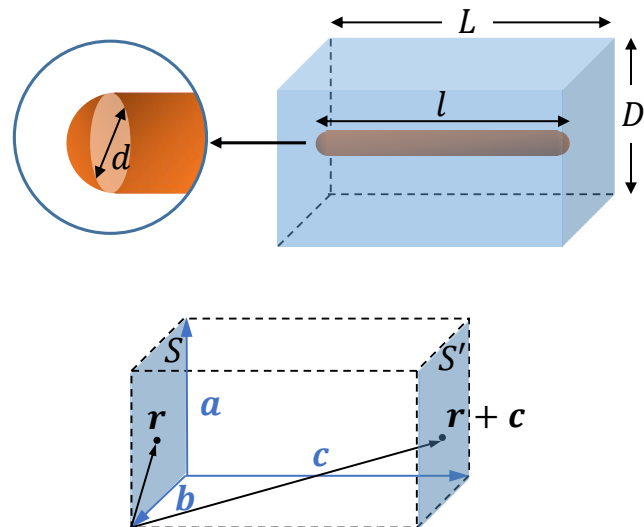


Fig. 4 Schematics of the model geometry and periodic boundary conditions in the finite element simulations. Top right: The unit cell in rectangular solid shape with one rigid fiber embedded. Top left: The smoothed end of the fiber using a semi-sphere with the same radius as the fiber's. The bottom illustration shows the correspondence between points on the opposite faces of a unit cell.

conditions require

$$\mathbf{u}(\mathbf{r} + \mathbf{c}) - \mathbf{u}(\mathbf{r}) = \mathbf{c}' - \mathbf{c} \quad (15)$$

which connects the local displacement vector of the unit cell with the global deformation of the lattice. In finite element simulations, the right-hand side of Eq. 15 is replaced with the displacement of a dummy node which is defined as

$$\mathbf{u}_{\mathbf{c}} = \mathbf{c}' - \mathbf{c} \quad (16)$$

In our model, $\mathbf{u}_{\mathbf{c}}$ is not prescribed *a priori* but determined by the contraction behavior of the fiber-reinforced hydrogel. Therefore, constraints among the two opposite faces and the dummy node are enforced in our simulations to solve $\mathbf{u}_{\mathbf{c}}$ according to Eq. 15 and 16. Similar constraints can also be derived for the other two pairs of opposite faces.

The periodic boundary conditions provide a simple and intuitive approach to investigate the anisotropic behavior of the hydrogel induced by the distributed fibers. However, it is worth mentioning that although previous experiments have verified the orientational long range order of the fibers, no periodicity is found in the positions of the fibers. Therefore, it is apparently an idealization to use the periodic boundary conditions in our simulations.

The unit cell in our simulations is modeled using a rectangular solid with $|\mathbf{a}| = |\mathbf{b}| = D$ and $|\mathbf{c}| = L$, as illustrated in the Fig. 4 (topright). Here we assume that the unit cell has identical periodicity in the directions of \mathbf{a} and \mathbf{b} . Within each unit cell, a cylindrical fiber is symmetrically placed in the center and oriented to the direction of \mathbf{c} ; thus L represents the longitudinal fiber-fiber distance, and the corresponding contraction ratio is α_{\parallel} . Likewise D should be equal to the transverse fiber-fiber distance; α_{\perp} is the

transverse contraction ratio as previously defined.

4.2 Constitutive model of hydrogel

We proceed to derive the constitutive model of the hydrogel within the context of finite element method. The thermodynamic equilibrium is achieved when the external work done on the hydrogel is equal to the change in the free energy:

$$\delta F = \int_V \delta \bar{F} dV = \int_V B_i \delta u_i dV + \int_S T_i \delta u_i dS \quad (17)$$

where \bar{F} is the nominal free energy density of the hydrogel, B_i is the external body force, T_i is the surface traction, and δu_i are arbitrary perturbation displacements. When the hydrogel reaches equilibrium, its chemical potential $\mu = \mu_{\text{external}} = 0$; thus in Eq. 17 we neglect the work done by the external chemical potential of the water.

Eq. 17 possesses the same form as a hyperelastic solid, which enables us to implement a finite element method for a hydrogel. In the context of continuum mechanics, it is traditional to formulate the free energy density \bar{F} in terms of the strain invariants:

$$I_1 = \lambda_1^2 + \lambda_2^2 + \lambda_3^2 \quad \text{and} \quad J = \lambda_1 \lambda_2 \lambda_3 = \phi^{-1} \quad (18)$$

Substituting Eq. 18 to 2 and 3 gives

$$\begin{aligned} \bar{F}(I_1, J, T) &= \frac{1}{2} \frac{N}{V_m} kT (I_1 - 3 - \ln J) \\ &+ \frac{kT}{\nu} \left[(J-1) \ln \left(1 - \frac{1}{J} \right) + \chi \left(1 - \frac{1}{J} \right) \right] \end{aligned} \quad (19)$$

Eq. 19 is singular at the molten state of the hydrogel ($J = 1$), which may lead to numerical problems if the molten state is involved in the calculations. To overcome this difficulty, we use an isotropic free swollen state with $J > 1$ as the reference state inspired by the study of Hong *et al.*³⁵. At this reference state, the hydrogel has isotropic stretching ratio λ_0 relative to the molten state. The volume fraction of the polymer is denoted by $\phi_0 = \lambda_0^{-3}$. Because the volume of the polymer V_m is assumed to be conserved, ϕ and ϕ_0 can be connected via

$$V\phi = V_0\phi_0 = V_m \quad (20)$$

where V_0 is the volume of the hydrogel at the reference state. The nominal free energy density \bar{F} and the strain invariants I_1, J are converted correspondingly to \bar{F}', I'_1, J' with respect to the new reference state:

$$\bar{F}(I_1, J, T) V_m = \bar{F}'(I'_1, J', T) V_0 \quad (21)$$

$$I_1 = \phi_0^{-2/3} I'_1 \quad \text{and} \quad J = \phi_0^{-1} J'$$

Substituting Eq. 20 and 21 to 19, we obtain that

$$\begin{aligned} \bar{F}'(I'_1, J', T) &= \frac{kT}{\nu} \left[\frac{1}{2} \frac{N\nu}{V_m} \phi_0 \left(\phi_0^{-2/3} I'_1 - 3 - \ln \frac{J'}{\phi_0} \right) \right. \\ &\left. + (J' - \phi_0) \ln \left(1 - \frac{\phi_0}{J'} \right) + \chi \phi_0 \left(1 - \frac{\phi_0}{J'} \right) \right] \end{aligned} \quad (22)$$

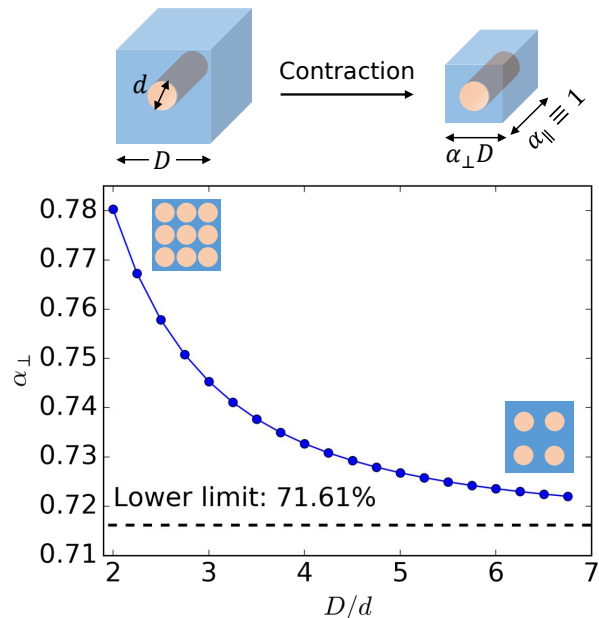


Fig. 5 The transverse contraction ratio of the fiber-reinforced hydrogel as a function of the transverse fiber-fiber distance at $L/l = 1$. The fiber is modeled as a regular cylindrical rod throughout the hydrogel matrix rather than a smoothed one to avoid possible numerical difficulties. The simulations are performed with $d = 10$ nm and $L = l = 30$ nm. The lower limit is calculated from the contraction of a uniaxially constrained hydrogel illustrated in Fig. 1a with the same set of parameters as used in the finite element simulations.

We implement the above constitutive model of the hydrogel by developing a user-defined subroutine for a hyperelastic material (UHYPER) in the commercial code ABAQUS. The contraction of the hydrogel is achieved by varying the value of χ calculated from Eq. 5 or 6. No prestretching is involved in our simulations, as we are focusing on the effects of the fiber dimensions; prestretching may also induce excessive deformations which lead to convergence difficulties. We set $\phi_i = \phi'_i = \phi_c = 0.125$ in the following simulations. The prescribed isotropic contraction ratio $\alpha_0 = 0.8$. $N\nu/V_m = 10^{-4}$ unless otherwise noted.

To verify our implementation, we numerically calculate the $\chi \sim \phi$ relations for both an isotropic swelling hydrogel and a uniaxially constrained hydrogel. (see supplementary Fig. S3) The results show perfect agreement with Eq. 5 and 6. In addition, the calculated uniaxial stress σ_3 for the uniaxially constrained hydrogel also coincides with Eq. 7 (see supplementary Fig. S3b).

4.3 Results and discussions

We firstly perform simulations for a limiting case where the fiber length is identical to the longitudinal length of the unit cell ($L/l = 1$), as shown in Fig. 5 (top). The hydrogel is therefore completely constrained along the orientation of the fibers ($\alpha_{\parallel} \equiv 1$). Simulations show that the transverse contraction ratio α_{\perp} decreases when increasing the transverse fiber-fiber distance (see Fig. 5 bottom). At small D/d , the transverse contraction of the hydrogel is highly restricted by the rigid cross-sections of the tightly packed fibers. This restriction become less significant as D/d in-

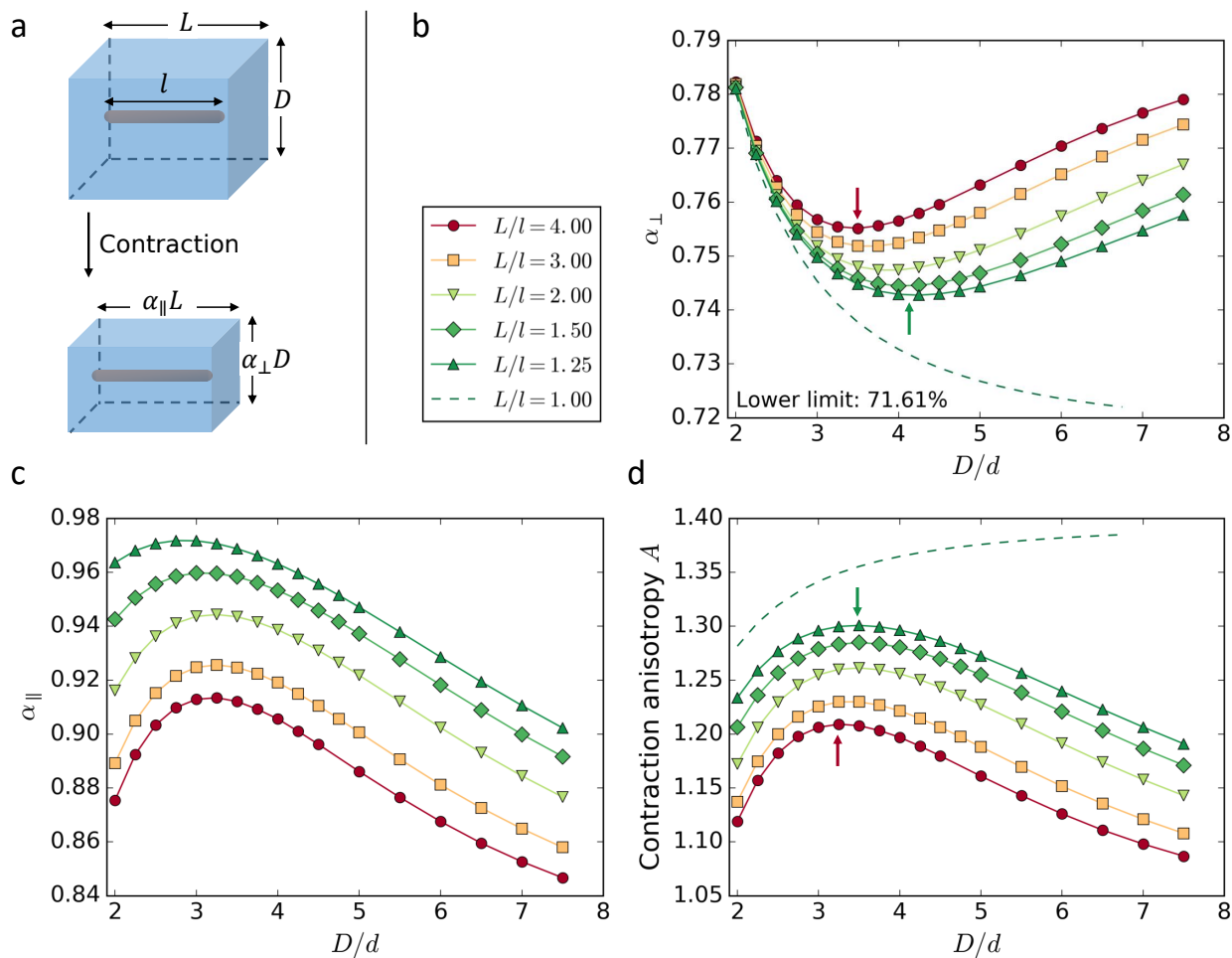


Fig. 6 The anisotropic contraction of the fiber-reinforced hydrogel at $L/l > 1.0$. (a) Schematic of the geometry to model the anisotropic contraction when $L > l$. (b-d) The transverse contraction ratio (b), the longitudinal contraction ratio (c) and the contraction anisotropy (d) as functions of the reduced transverse fiber-fiber distance (D/d). The data for $L/l = 1$ in (b) (dashed curves) are identical to Fig. 5 as $\alpha_{\parallel} \equiv 1$. The arrows in both (b) and (d) indicate the shifts of the minimum α_{\perp} and the maximum A . The legend in (b) is also shared by (c) and (d). All the simulations are performed with $d = 10$ nm and $l = 200$ nm.

creases, hence leading to stronger transverse contraction and decreasing α_{\perp} . Eventually, the transverse dimensions of the fibers is negligible so that the hydrogel behaves as if it were uniaxially constrained without fibers embedded. Thus, α_{\perp} converges to a lower limit that can be predicted from the uniaxially constrained hydrogel model discussed in previous sections. We also conduct similar simulations for a prestretching fiber-reinforced hydrogel; same behaviors of α_{\perp} are found in the supplementary Fig. S4.

Intuitively, however, an infinitely large hydrogel with few fibers embedded (i.e., $D \gg d$) should shrink almost isotropically upon external stimuli, which can never be captured in the above simulations by assuming $L/l = 1$ and $\alpha_{\parallel} \equiv 1$. Therefore, we proceed to investigate the anisotropic contraction at $L/l > 1$ which allows the hydrogel to shrink longitudinally (see Fig. 6a). Figure 6b shows that the transverse contraction ratio α_{\perp} has a minimum for each L/l , whereas α_{\parallel} exhibits the opposite behavior (Fig. 6c). These results can be understood as follows. At small D/d , the transverse contraction can be significantly amplified by releasing the aforementioned restrictions from the rigid cross-sections of the fibers. In contrast, the longitudinal contraction is energetically disfavored due to the induced stress concentration near the ends of the fibers (see supplementary Fig. S5); meanwhile it is also restricted by the rigid length of the fibers. Consequently, α_{\perp} exhibits rapid decrease at small D/d where increasing α_{\parallel} is observed. When D/d becomes noticeably larger, both α_{\perp} and α_{\parallel} vary in the opposite way compared to the previous case. Stronger longitudinal contraction is instead preferred at large D/d when the fibers are more sparsely distributed: the bulky hydrogel far from the fibers can undergo less longitudinal strain, thus mediating the local stress concentration near the fibers.

The anisotropy of the hydrogel contraction ($A \equiv \alpha_{\parallel}/\alpha_{\perp}$) can be evaluated from Fig. 6b and 6c. As shown in Fig. 6d, A presents a maximum for each L/l , just as expected based on the behavior of α_{\parallel} in Fig. 6c. A shift of the maxima toward higher D/d with decreasing L/l is observed in both Fig. 6b and Fig. 6d. Indeed, the stronger constraint from the fibers at lower L/l need to be balanced out with larger longitudinal contraction induced by increasing D/d , thus the optimum D/d increases when reducing L/l . Besides, we have also inspected the contraction anisotropies at different Nv/V_m , a dimensionless parameter characterizing the rigidity of the hydrogel; the maxima therein do not show any shift along the D/d axis (see supplementary Fig. S6). Additionally, A is observed to be enhanced at lower L/l in Fig. 6d. This increasing anisotropy stems from the dampening of the longitudinal contraction when decreasing L/l ; the longitudinal separation of the fibers is reduced such that the hydrogel has less freedom to shrink along the longitudinal direction. Overall, we conclude that the contraction anisotropy can be maximized by adjusting the transverse fiber-fiber distance D/d , and this maximum value can be further elevated by reducing the longitudinal fiber-fiber distance L/l .

Our simulations also reveal that fibers with larger aspect ratio (l/d) can lead to stronger anisotropy of the hydrogel contractions. Note that L/l is kept as a constant for different l/d such that same portion of the hydrogel is restricted by the rigid fibers. Figure 7 clearly shows that A decreases with increasing l/d . More

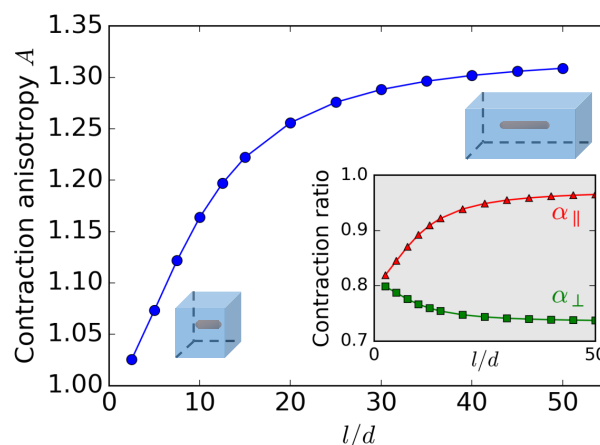


Fig. 7 The contraction anisotropy of the fiber-reinforced hydrogel as a function of the shape aspect ratio of the fiber (l/d). $L/l = 2.0$. The corresponding transverse contraction ratio (α_{\perp} , green line) and longitudinal contraction ratio (α_{\parallel} , red line) are depicted in the inset. The simulations are performed with $d = 10$ nm and $D = 40$ nm.

particularly, as depicted in the inset of Fig. 7, α_{\parallel} exhibits a significant increase: at $l/d = 5$, it is only slightly larger than $\alpha_0 = 0.8$, whereas it reaches ~ 0.96 when l/d increases to 50. The substantial increase of α_{\parallel} at constant L/l implies that longer fibers can enforce much stronger longitudinal constraints on the hydrogel, thus facilitating the anisotropic contraction. This observation has been validated in former experiments^{9,23} where fibers with a high aspect ratio ($l/d > 100$) are indeed adopted to achieve high anisotropy. We note that in Ref.²³, the overall mass ratio of the fibers is 0.7%, the length of fibers in the supramolecular hybrid hydrogel is more than 400 times of the fiber radius, and the transverse fiber-fiber distance is roughly 10 times of the fiber radius. As a result, the constraint from the fibers plays an important role in causing the strongly anisotropic contraction of the hybrid hydrogel, as predicted by our finite element simulations (see Fig. 7). These experimental parameters are indeed close to the limiting case studied in our previous theoretical model (in section 3), which essentially neglects the transverse dimension of the fibers, and assumes that they are long enough to prevent the longitudinal contraction. Therefore, although the longitudinal contraction cannot be completely restricted in reality, it is still possible to achieve strong longitudinal constraint by increasing the fiber length even if the transverse density of fibers is low, leading to a high contraction anisotropy.

It is worth mentioning that our finite element model is developed based on several assumptions that significantly simplify the realistic fiber-reinforced hydrogel systems. For example, the oriented fibers in our model are arranged as a periodic lattice, while experimentally they usually do not have long-range translational order. Experiments also show that long fibers can bend and twist rather than keep absolutely straight in the hydrogel matrix²¹. In addition, the interactions between the fibers, which are absent in our simulations, may also play an important role in the contraction of the whole hydrogel system. Besides, prestretching is problematic in our simulations with finite-length fibers, due

to the complex interplay between the prestretching stress, fiber constraint and the isotropic contraction of the hydrogel matrix. More sophisticated numerical methods are required to handle extremely large deformations of the elements that may lead to convergence difficulties. Despite all these limitations, our simple finite element model provides a reference point for more sophisticated models. We stress that the variation trend of the contraction anisotropy at the limit of both the small and large transverse fiber-fiber distance should still be valid when the above complexities are considered.

5 Conclusions

This study focuses on the mechanisms controlling the anisotropic contraction of a fiber-reinforced hydrogel. By idealizing the reinforcement of the fibers as a uniaxial constraint, and assuming χ is independent of ϕ , we discover that the contraction anisotropy has an upper bound determined by the prescribed isotropic contraction. Numerical analysis of the $\chi \sim \phi$ relations further reveals that it is possible to exceed this limit by introducing longitudinal prestretching into the hydrogel; such mechanism also applies for certain practical systems with ϕ -dependent χ such as PEO hydrogels. Assuming the fibers are rigid and periodically distributed, finite element simulations show that the contraction anisotropy can be maximized by varying the transverse fiber-fiber distance; this maximum value can be further improved by reducing the longitudinal fiber-fiber distance or increasing the fiber length, both of which essentially strengthen the longitudinal constraint of the fibers. These findings provide insights into designing fiber-reinforced hydrogels with desired anisotropic behavior under various stimuli, which can be applicable in soft robotics, tissue engineering and so on. Future studies are needed to elucidate the potential impact of other important factors on the anisotropic contraction, including the deformability of fibers, different fiber arrangements and interactions between fibers and the hydrogel matrix.

Acknowledgements

The research was supported by the Center for Bio-Inspired Energy Science, an Energy Frontier Research Center funded by the U.S. Department of Energy (DOE), Office of Science, Basic Energy Sciences (BES), under Award DE-SC0000989

References

- 1 Y. Li and T. Tanaka, *Annual Review of Materials Science*, 1992, **22**, 243–277.
- 2 M. C. Koetting, J. T. Peters, S. D. Steichen and N. A. Peppas, *Materials Science and Engineering: R: Reports*, 2015, **93**, 1–49.
- 3 A. S. Hoffman, *Advanced Drug Delivery Reviews*, 2012, **64**, 18–23.
- 4 V. Chan, K. Park, M. B. Collens, H. Kong, T. A. Saif and R. Bashir, *Scientific Reports*, 2012, **2**, 857.
- 5 L. Ionov, *Materials Today*, 2014, **17**, 494–503.
- 6 T. R. Hoare and D. S. Kohane, *Polymer*, 2008, **49**, 1993–2007.
- 7 A. Richter, G. Paschew, S. Klatt, J. Lienig, K.-F. Arndt and H.-J. P. Adler, *Sensors*, 2008, **8**, 561–581.
- 8 J.-Y. Sun, C. Keplinger, G. M. Whitesides and Z. Suo, *Advanced Materials*, 2014, **26**, 7608–7614.
- 9 A. S. Gladman, E. A. Matsumoto, R. G. Nuzzo, L. Mahadevan and J. A. Lewis, *Nature Materials*, 2016, **15**, 413–418.
- 10 M. Rafat, F. Li, P. Fagerholm, N. S. Lagali, M. A. Watsky, R. Munger, T. Matsuura and M. Griffith, *Biomaterials*, 2008, **29**, 3960–3972.
- 11 C.-D. Young, J.-R. Wu and T.-L. Tsou, *Biomaterials*, 1998, **19**, 1745–1752.
- 12 J. L. Drury and D. J. Mooney, *Biomaterials*, 2003, **24**, 4337–4351.
- 13 T. Dvir, B. P. Timko, M. D. Brigham, S. R. Naik, S. S. Karajanagi, O. Levy, H. Jin, K. K. Parker, R. Langer and D. S. Kohane, *Nature Nanotechnology*, 2011, **6**, 720–725.
- 14 A. Agrawal, N. Rahbar and P. D. Calvert, *Acta Biomaterialia*, 2013, **9**, 5313–5318.
- 15 F. T. Moutos, L. E. Freed and F. Guilak, *Nature Materials*, 2007, **6**, 162–167.
- 16 Y. S. Kim, M. Liu, Y. Ishida, Y. Ebina, M. Osada, T. Sasaki, T. Hikima, M. Takata and T. Aida, *Nature Materials*, 2015, **14**, 1002–1007.
- 17 S. Ahadian, J. Ramón-Azcón, M. Estili, X. Liang, S. Ostrovidov, H. Shiku, M. Ramalingam, K. Nakajima, Y. Sakka, H. Bae, T. Matsue and A. Khademhosseini, *Scientific reports*, 2014, **4**, 4271.
- 18 M. A. Haque, G. Kamita, T. Kurokawa, K. Tsujii and J. P. Gong, *Advanced Materials*, 2010, **22**, 5110–5114.
- 19 M. Chau, K. J. France, B. Kopera, V. R. Machado, S. Rosenfeldt, L. Reyes, K. J. Chan, S. Förster, E. D. Cranston, T. Hoare and E. Kumacheva, *Chemistry of Materials*, 2016, **28**, 3406–3415.
- 20 L. Zhang, J. B. Bailey, R. H. Subramanian and F. A. Tezcan, *Nature*, 2018, **557**, 86–91.
- 21 M. T. McClendon and S. I. Stupp, 2012, **33**, 5713–5722.
- 22 J. Visser, F. P. Melchels, J. E. Jeon, E. M. v. Bussel, L. S. Kimp-ton, H. M. Byrne, W. J. Dhert, P. D. Dalton, D. W. Huttmacher and J. Malda, *Nature Communications*, 2015, **6**, 6933.
- 23 S. M. Chin, C. V. Synatschke, S. Liu, R. J. Nap, N. A. Sather, Q. Wang, Z. Álvarez, A. N. Edelbrock, T. Fyrner, L. C. Palmer, I. Szeleifer, M. O. d. l. Cruz and S. I. Stupp, *Nature Communications*, 2018, **9**, 2395.
- 24 J. Merodio and R. Ogden, *International Journal of Non-Linear Mechanics*, 2005, **40**, 213–227.
- 25 P. Nardinocchi, M. Pezzulla and L. Teresi, *Soft matter*, 2015, **11**, 1492–1499.
- 26 Y. Liu, H. Zhang, J. Zhang and Y. Zheng, *European Journal of Mechanics - A/Solids*, 2015, **54**, 171–186.
- 27 P. J. Flory and J. Rehner, 1943, **11**, 512.
- 28 F. T. Wall and P. J. Flory, *The Journal of Chemical Physics*, 1951, **19**, 1435–1439.
- 29 L. Anand, *Computational Mechanics*, 1996, **18**, 339–355.
- 30 M. C. Boyce and E. M. Arruda, *Rubber Chemistry and Technology*, 2000, **73**, 504–523.
- 31 P. J. Flory, *Principles of polymer chemistry*, 1953, p. 672.

- 32 M. L. Huggins, *Journal of the American Chemical Society*, 1964, **86**, 3535–3540.
- 33 Y. C. Bae, S. M. Lambert, D. S. Soane and J. M. Prausnitz, *Macromolecules*, 1991, **24**, 4403–4407.
- 34 E. E. Dormidontova, *Macromolecules*, 2002, **35**, 987–1001.
- 35 W. Hong, Z. Liu and Z. Suo, *International Journal of Solids and Structures*, 2009, **46**, 3282–3289.
- 36 R. Marcombe, S. Cai, W. Hong, X. Zhao, Y. Lapusta and Z. Suo, *Soft Matter*, 2010, **6**, 784–793.
- 37 S. A. Chester and L. Anand, *Journal of the Mechanics and Physics of Solids*, 2010, **58**, 1879–1906.
- 38 D. Li, Z. Zhang and K. Liew, *Computer Methods in Applied Mechanics and Engineering*, 2014, **274**, 84–102.
- 39 M. Quesada-Pérez, J. Ramos, J. Forcada and A. Martín-Molina, *The Journal of chemical physics*, 2012, **136**, 244903.
- 40 Z. Ding, Z. Liu, J. Hu, S. Swaddiwudhipong and Z. Yang, *International Journal of Solids and Structures*, 2013, **50**, 2610–2619.
- 41 D. Okumura, T. Kuwayama and N. Ohno, *International Journal of Solids and Structures*, 2014, **51**, 154–163.
- 42 H. Lee, J. Zhang, H. Jiang and N. X. Fang, *Physical Review Letters*, 2012, **108**, 214304.
- 43 F. Weiss, S. Cai, Y. Hu, M. K. Kang, R. Huang and Z. Suo, *Journal of Applied Physics*, 2013, **114**, 073507.

The contraction anisotropy of a fiber-reinforced hydrogel can be improved by applying pre-stretch and optimizing the transverse fiber-fiber distance.

